Polymer Chemistry

PAPER

View Article Online
View Journal | View Issue

Cite this: *Polym. Chem.*, 2016, **7**, 7249

Stress-sensing thermoset polymer networks *via* grafted cinnamoyl/cyclobutane mechanophore units in epoxy

Elizabeth M. Nofen, Nicholas Zimmer, Avi Dasgupta, Ryan Gunckel, Bonsung Koo, Aditi Chattopadhyay and Lenore L. Dai*

The incorporation of mechanophores into networked thermoset polymers, such as epoxy, is notably missing from the mechanochemistry literature, which focuses more on traditional thermoplastic and elastomeric polymers. In this work, we develop novel approaches for direct covalent grafting of photoactive mechanophore units into an epoxy matrix (a two-part network polymer), to create a self-sensing thermoset network nanocomposite, linked by both epoxide and mechanophore bonds. Two routes of grafting mechanophore units into an epoxy system to form a self-sensing nanocomposite were explored, including grafting of the mechanophore precursor molecule cinnamamide to the epoxy resin, with subsequent hardener addition and ultraviolet curing to form the mechanically sensitive cyclobutane rings, and the separate grafting of the solution-made mechanophore di-cinnamamide to the epoxy resin to allow for maximum cyclobutane concentration in the formed nanocomposites. Under a compressive force, the cyclobutane rings in the mechanophore units break, increasing the overall fluorescence, which can then be correlated with the applied stress. The goals of this work included detecting early damage by fluorescence spectroscopy, environmental robustness, and retention of the mechanical and thermal properties of the composite. Overall, there was successful formation of self-sensing nanocomposites and achievement of the early damage detection functionality. This systematic work additionally aims to provide further fundamental understanding of mechanochemistry as a whole.

Received 22nd August 2016,
Accepted 16th October 2016

DOI: 10.1039/c6py01463a

www.rsc.org/polymers

1. Introduction

Mechanochemistry encompasses the use of mechanical force to induce a chemical change, with early studies focusing on the type of mechanical force applied, such as ball milling and grinding, and to realize reaction pathways not possible *via* alternative means.[1–3] In the recent years, the focus of the field has shifted towards utilizing mechanochemistry as a tool to probe the local mechanical environment of chemical bonds, with the development of specialized force-responsive molecular units, or mechanophores.[4–6] Mechanophores undergo selective bond scission in response to an external force to provide a measureable signal to correlate with the applied force for a targeted chemical response.[7–9] The examples of mechanophore bond scission include targeted homolytic cleavage, dative bond scission, cycloreversion, and electrocyclic ring opening.[10] Mechanophores are often also mechanochromic, or change color with an applied force, showing a visible light or fluorescent response to a mechanical force.[11–14] The responsiveness and tunability of mechanophores thus lead to the relatively new and exciting field of polymer mechanochemistry.[15–17]

An important breakthrough in the polymer mechanochemistry field was the synthesis of spiropyran (SP)-embedded, elastomeric poly(methyl acrylate) (PMA) chains, with the SP units acting as force sensors in response to tensile loading.[6] Tensile testing and simultaneous optical spectroscopy were applied to examine the force-induced 6-electrocyclic ring-opening reaction from colorless spiropyran to colored merocyanine, resulting in a mechanically induced visible color change. The researchers additionally showed that SP could act as a functional mechanophore crosslinker in glassy poly(methyl methacrylate) (PMMA) beads.[6] As the mechanically induced signal from SP is visible to the naked eye, other researchers have used it as their mechanophore of choice in various elastomeric or thermoplastic polymer systems, including as crosslinkers in PMMA,[18] in rubber-toughened PMMA,[19] and in networked elastomeric poly(dimethylsiloxane) (PDMS).[20]

Cycloaddition *via* photodimerization is a well-known mechanism, in which certain monomeric structures can dimerize

School for Engineering of Matter, Transport and Energy, Arizona State University, Tempe, Arizona 85287, USA. E-mail: lenore.dai@asu.edu; Fax: +1 480 727 9321; Tel: +1 480 965 4112

into cycloalkane rings, such as cinnamoyl groups into cyclobutane *via* [2 + 2] cycloaddition.[21,22] Cyclobutane rings formed from the photodimerization of cinnamoyl groups can also act as mechanophore units, with the strained rings reverting to their fluorescent, monomeric cinnamoyl form after an applied stress.[23–25] The strained cyclobutane ring structure has been used as a mechanophore in a number of studies, including to produce a mendable poly(butylene adipate) network by functionalization with cinnamoyl groups,[26] as masked cyanoacrylate functional groups,[27] and as various mono- and di-cyano-substituted (and without cyano groups) cyclobutanes to study the collapse of cavitation bubbles.[28,29]

While many studies regarding thermoplastic and elastomeric polymer mechanochemistry exist, there has been limited study of mechanochemistry within another branch of polymer chemistry, that being thermoset network polymers.[8,16,17] Thermosets find ubiquitous use due to their excellent mechanical and physical properties, including in printed circuit boards, high-performance adhesives, military personal protective equipment, and various marine, aerospace, and other applications.[30–33] Cured epoxy resins are generally quite brittle, with a propensity to crack if exposed to sufficient stress and strain, leading to irreversible damage such as microcracking.[34–36] When mechanophores are incorporated into the backbone of linear, thermoplastic or elastomeric polymers, the mechanophore activation in these systems requires a relatively large deformation.[37] Additionally, when a mechanophore is incorporated into polymer chains, it requires an appropriate position relative to the polymer backbone, because mechanophores can only be force-activated if the force can be effectively transferred through the bulk material to individual chains, then to the cleavable bonds on the mechanophore units.[38] While mechanically sensitive retro Diels–Alder reactions have been studied in thermoplastic elastomeric systems,[20,39–41] thermally responsive Diels–Alder adducts have only been applied in thermoset networks for a self-healing functionality,[42–44] with force-responsive thermoset networks not currently seen in the literature. The networked polymer nature of thermosets thus provides a unique platform to study mechanochemistry, due to their ubiquitous use, superior physical properties, and unique molecular architecture.

Mechanochemistry allows for the development and employment of unique stress-responsive materials targeted towards damage monitoring and recovering damage.[45] In our previous work, we applied mechanochemistry to thermoset systems by creating self-sensing polymer blends of cyclobutane-based mechanophores and epoxy.[46] We then followed up the work by synthesizing dimeric anthracene-based mechanophore particles and applying them to an epoxy matrix for damage precursor detection.[47] However, when the mechanophores were simply used as stress-sensing additives, the self-sensing could only occur between the stress-sensing molecules, and any damage done to the matrix polymer could not be sensed, the fluorescent nature only serving as a signal to the damage. Another notable drawback of utilizing mechanophores as additives was the significant lowering of the glass transition temperature of the system, narrowing the temperature window in which the composite can be used. Thus, we propose to overcome these limitations by direct covalent incorporation of the mechanophore units into an epoxy network thermoset polymer to create a novel functionalized nanocomposite system, by using the mechanophore precursor and mechanophore, cinnamamide and di-cinnamamide, respectively. This systematic and novel work also provided further fundamental understanding of mechanochemistry as a whole.

2. Experimental

2.1. Materials

Cinnamamide (Cinn, Sigma-Aldrich), diethyl ether (VWR International), and deuterated dimethyl sulfoxide (DMSO-d_6, Cambridge Isotope Laboratories) were used as received. The epoxy resin FS-A23 (digycidylether of bisphenol F, DGEBPF) and epoxy hardener FS-B412 (diethylenetriamine, DETA) were purchased from Epoxy Systems Inc. and used as received.

2.2. Synthesis of dimeric cinnamamide (Di-Cinn) and chemical characterization

To synthesize di-cinnamamide, 2 g of cinnamamide were dissolved in 40 mL of diethyl ether and the mixture was homogenized *via* magnetic stirring and under a nitrogen purge. The solution was then photoirradiated with a 302 nm wavelength UV lamp (UVP, UVM-28), with a light density of approximately 1300 μW cm^{-2} at a distance of 3 cm, for two days. A white precipitate was formed, which was washed with diethyl ether by gravity filtration to remove the brown cinnamamide monomer, until the bottom solution was clear. The product was then dried to remove the excess solvent. ^{1}H NMR (400 MHz, DMSO-d_6) δ 7.53–7.07 (10H, m), 6.55 (4H, d), 3.29 (4H, s).

^{1}H Nuclear Magnetic Resonance (NMR) spectra were recorded with a Bruker 400 MHz NMR spectrometer. For the NMR samples, approximately 5 mg of the sample was dissolved in 750 μL of DMSO-d_6. Fourier Transform Infrared (FTIR) spectra were recorded under vacuum using a Bruker IFS 66v/S FTIR spectrometer equipped with a Pike Diamond ATR (Attenuated Total Reflectance) accessory. Emission spectra were recorded with a Horiba Scientific FluoroLog-3 Spectrofluorometer with an excitation wavelength of 350 nm, and all slits set at 1 nm. Microscopic morphologies of the surface of the epoxy samples were taken with a FEI/Philips XL30 Environmental FEG Scanning Electron Microscope (SEM). The chemical structures were drawn with MarvinSketch.

2.3. Preparation and characterization of mechanophore-embedded epoxy matrix composites

To form the studied nanocomposites consisting of 10 wt% cinnamamide or 10 wt% di-cinnamamide in 5 g total epoxy, each was first reacted with the resin to ensure the covalent bond formation. 0.5 g of cinnamamide or di-cinnamamide was added to 3.704 g of epoxy resin (digycidylether of bisphenol F,

DGEBPF) and 20 mL of dichloromethane. This mixture was then heated at 40 °C for 4 h under a nitrogen purge and magnetic stirring to allow for the reaction between the epoxide rings and the amine groups. After the reaction was complete, the cinnamamide reaction solution turned fluorescent opaque yellow while the di-cinnamamide reaction solution was white and opaque. The dichloromethane solvent was then removed under reduced pressure and 0.796 g of hardener (diethylenetriamine, DETA) was added to each functionalized resin mixture (4.204 g total). The hardener/resin/mechanophore weight ratio was calculated according to the manufacturer's recommendations and the epoxide/amine equivalent weight. These mixtures were then impeller-mixed at 200 rpm for 5 min at room temperature until homogeneous. The mixtures were then poured into silicone rubber molds, sprayed with a mold release agent and allowed to cure overnight at room temperature, with the cinnamamide epoxy being UV cured for 4 h under 365 nm light (UVP, UVLMS-38) prior to leaving in darkness to complete the curing. Neat epoxy samples were prepared in a similar manner with a 100 : 27 ratio of resin to hardener.

After simple machining, the average dimensions of the samples for the compression test were 3 × 4 × 8 mm and 2 × 12 × 35 mm for the Dynamic Mechanical Analyzer (DMA) tests. A TA Instruments Q20 Differential Scanning Calorimeter (DSC) was used to determine the glass transition temperature (T_g) of the epoxy samples in aluminum Tzero pans with lids under nitrogen, with air (an empty pan and lid) used as the reference. The sample was first heated to 70 °C to eliminate any thermal history, cooled down to −20 °C, and then heated to 120 °C to determine the T_g, with all heating and cooling rates set at 10 °C min^{-1}. A TA Instruments Thermogravimetric Analyzer (TGA) Q500 was used to determine the decomposition temperatures (T_d) under nitrogen. Each sample was placed in a tared platinum crucible and heated from 25 to 600 °C at a heating rate of 10 °C min^{-1}. A TA Instruments Q800 Dynamic Mechanical Analyzer (DMA) was used to measure the storage modulus, loss modulus, and tan delta for the epoxy samples over a temperature range and to calculate the crosslink density. The multi-frequency/strain method was used with the single cantilever clamp and a frequency of 1 Hz under amplitude control. The temperature was ramped from 25 to 120 °C at a heating rate of 5 °C min^{-1}, with the strain amplitude set at 25 μm. The characteristic temperatures and moduli values from DSC, TGA, and DMA were found using the built-in functions in the TA Instruments Universal Analysis software. A TestResources 800L Compression Test System was used to compress the samples to different strains and obtain stress–strain plots for the epoxy samples. A small amount of petroleum jelly was applied to the samples to minimize their friction with the compression plate, and prevent unwanted shearing. The tests were run in displacement control in the longitudinal direction at a loading rate of 1 mm min^{-1} and conducted at room temperature. The fluorescence generation from the compressed epoxy samples was observed under a Nikon Eclipse TE300 inverted video fluorescence microscope, by excitation under 340–380 nm UV light, with a filter cube to capture the emission of light between 500–550 nm. All images were taken with a black-and-white camera and with the same intensity of light, gain, and exposure time. The ImageJ (http://imagej.nih.gov/ij/) software package was used to quantify the fluorescence intensity of the images taken. Every image was first converted to an 8-bit image and then the "Measure" function was used to calculate the integrated intensity for the selected area of the image; this is through the software taking the sum of the pixel values in the image, and then averaging the intensity at each point. The 8-bit gray scale fluorescence images from the fluorescence microscope were subsequently pseudocolored green with ImageJ with the built-in "Green" LUT, and the fluorescence images published in this paper were all further enhanced by increasing both brightness and contrast by 40% for better viewing.

3. Results and discussion

3.1. Formation of the mechanophore-grafted self-sensing thermoset network polymer

For this study, the mechanophore precursor chosen was cinnamamide (Cinn, chemical structure in Fig. 1b left inset), as it is commercially available and its amine group can covalently bond to the epoxy resin chosen (diglycidyl ether of bisphenol F, DGEBF), in a similar manner to the crosslinking of the resin with the chosen hardener (diethylenetriamine, DETA) in the neat epoxy system. Cinnamamide is known to be able to form a cyclobutane type dimer (di cinnamamide, Di-Cinn, chemical structure in Fig. 1c left inset) under UV photoirradiation *via* [2 + 2] cycloaddition. Thus two routes are studied in this work for the mechanophore covalent incorporation into an epoxy matrix, the first being the reaction of the cinnamamide mechanophore precursor with DGEBF to ensure covalent bond formation, with subsequent hardener addition.

The epoxy mixture is then UV cured so that the cyclobutane mechanophore units can be formed *via* photodimerization, while the conventional resin-hardener curing is taking place. The second route is to first form di-cinnamamide in solution under UV light, then to react it with DGEBF, with subsequent hardener addition and conventional epoxy bond formation. In this second method, it was expected that more cyclobutane rings would be present in the final nanocomposite, as Di-Cinn is theoretically 100% dimerized prior to addition, and was confirmed *via* the amount of initial fluorescence of the composite for the same weight percentage of the mechanophore used. In this route, the penetration depth for curing an epoxy sample and the UV curing efficiency do not play a role. In the Cinn-containing composite, this dimerization occurs in the viscous epoxy resin-hardener solution, and thus there is competition between the two types of crosslink formation as well as physical impedance for the cinnamoyl groups to find each other in the mixture and dimerize, compared to simple dimerization in solution.

To form the studied nanocomposites, the cinnamamide dimer was first synthesized by dissolving cinnamamide in

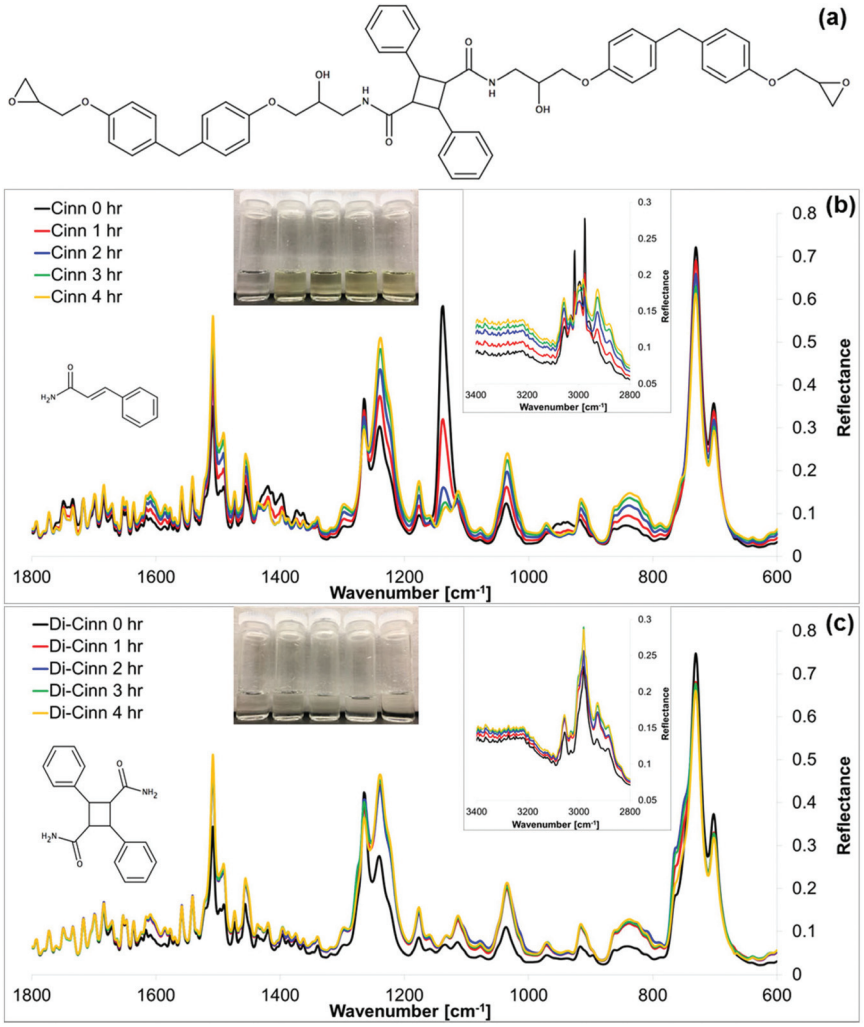

Fig. 1 (a) Chemical structure of a cinnamamide dimer di-substituted with the epoxy resin diglycidyl ether of bisphenol F. (b) ATR-FTIR spectra for the reaction of cinnamamide (chemical structure in the left inset) with DGEBF over reaction time; inset, macroscopic image of the reaction solution over reaction time; inset, ATR-FTIR spectra of the region between 3400 and 2900 cm^{-1}. (c) ATR-FTIR spectra for the reaction of di-cinnamamide (chemical structure in the left inset) with DGEBF over reaction time; inset, macroscopic image of the reaction solution over reaction time; inset, ATR-FTIR spectra of the region between 3400 and 2900 cm^{-1}.

diethyl ether under magnetic stirring and a nitrogen purge. The solution was then photoirradiated with a 302 nm wavelength UV lamp for two days to carry out the [2 + 2] cycloaddition for the formation of the cyclobutane rings. The white Di-Cinn precipitate was then washed and dried to obtain a pure product. To form the studied nanocomposites consisting of covalently bonded 10 wt% cinnamamide or 10 wt% di-cinnamamide in epoxy, each was first reacted with the resin to ensure the covalent bond formation between the amine hydrogens in Cinn or Di-Cinn and the epoxide rings of DGEBF. This was performed by adding cinnamamide or di-cinnamamide to DGEBPF with dichloromethane as a solvent. This mixture was then heated at 40 °C for 4 h under a nitrogen purge and magnetic stirring to promote the reaction between the epoxide rings and the amine groups. The dichloromethane solvent was then removed under reduced pressure and the diethylenetriamine hardener was added to each functionalized resin mixture, with the hardener/resin/mechanophore weight ratio calculated according to the manufacturer's recommendations and the epoxide/amine equivalent weight. The amount of mechanophore *vs.* epoxide crosslinks must be balanced in order to allow for the desired sensing signal while not depressing the thermal and mechanical properties of the matrix. These mixtures were then impeller-mixed at room temperature until homogeneous, subsequently poured into silicone rubber molds and allowed to cure overnight at room temperature, with the cinnamamide epoxy being UV cured for 4 h under 365 nm light prior to leaving in darkness to complete the curing. Neat epoxy samples were prepared in a similar manner with a 100 : 27 ratio of resin to hardener.

The chemical structure in Fig. 1a shows a cinnamamide dimer di-substituted with DGEBF, with the resin containing two active epoxide ring end groups that can covalently bond with an amine hydrogen active site. Theoretically, each amine

from a cinnamamide group has two free active hydrogen sites that could participate in this reaction (with a total of 4 for a di-cinnamamide molecule), but as seen in Fig. 1a, sterical hindrance of the reaction should be taken into account. Because the cinnamamide or di-cinnamamide first reacts with the resin molecule, there is a higher probability for increased covalent bonding to occur (compared to the reaction happening in the epoxy *in situ*), however there is likely a higher substitution occurring with cinnamamide compared to di-cinnamamide, due to the steric hindrance. Thus, to evaluate the amount of substitution, ATR-FTIR was performed on the reaction solutions of cinnamamide/di-cinnamamide and DGEBF in dichloromethane, as seen in Fig. 1b and c, respectively. Interestingly, in the reaction solutions for either chemistry, the primary amine hydrogen peaks representative of Cinn and Di-Cinn at 3367 and 3157 cm^{-1} (seen in Fig. 2a) are not present in the FTIR scans. However, there are other important functional group peaks present to evaluate the mechanophore–resin grafting over the reaction time. As the ATR-FTIR accessory was used on these samples, quantitative analysis regarding the change in peak height over the reaction time can be made. For both the cinnamamide– and di-cinnamamide–resin reaction FTIR spectra shown in Fig. 1b and c, important functional group peak changes over reaction time include a slight reduction of the 730 and 700 cm^{-1} peaks for the aromatic C–H bend, attributed to the change in aromaticity upon grafting; the dramatic increase of the peak at 1032 cm^{-1}, for the formation of new C–OH bonds upon opening of the epoxide rings; an increase at 1175 cm^{-1}, again for the new C–OH stretch; a dramatic increase near 1237 cm^{-1} for the for the C–O–C ether stretch in DGEBF change in conjugation; a decrease at 1265 cm^{-1} for the removal of the C–O stretch in the epoxides; an increase at 1454 cm^{-1} for the C–H aliphatic hydrogens; and increases at 1490, 1508, and 1606 cm^{-1} for the benzene ring, due to its change in conjugation over the reaction time. In only the cinnamamide–resin reaction FTIR spectra, there is a dramatic reduction of the peak at 1140 cm^{-1}, which can be correlated with the loss of the C–N amine peak, specifically for primary amines.[48–51]

In the inset spectra in Fig. 1b and c showing the wavenumbers from 3400 and 2900 cm^{-1}, there is an overlaying of the peaks for the C–H bonds of the aromatics, alkanes, and epoxide rings. For both cinnamamide and di-cinnamamide, there is an increase of the 3055, 2980, and 2924 cm^{-1} peaks, and for cinnamamide, there is a clear removal of the 2976 and 3015 cm^{-1} peaks after the reaction is completed. As the conjugation and interactions of the molecules can obscure the specific identification of these peaks, the simple change in peak intensity and the removal of certain peaks in this region will provide the additional evidence of the procession of the

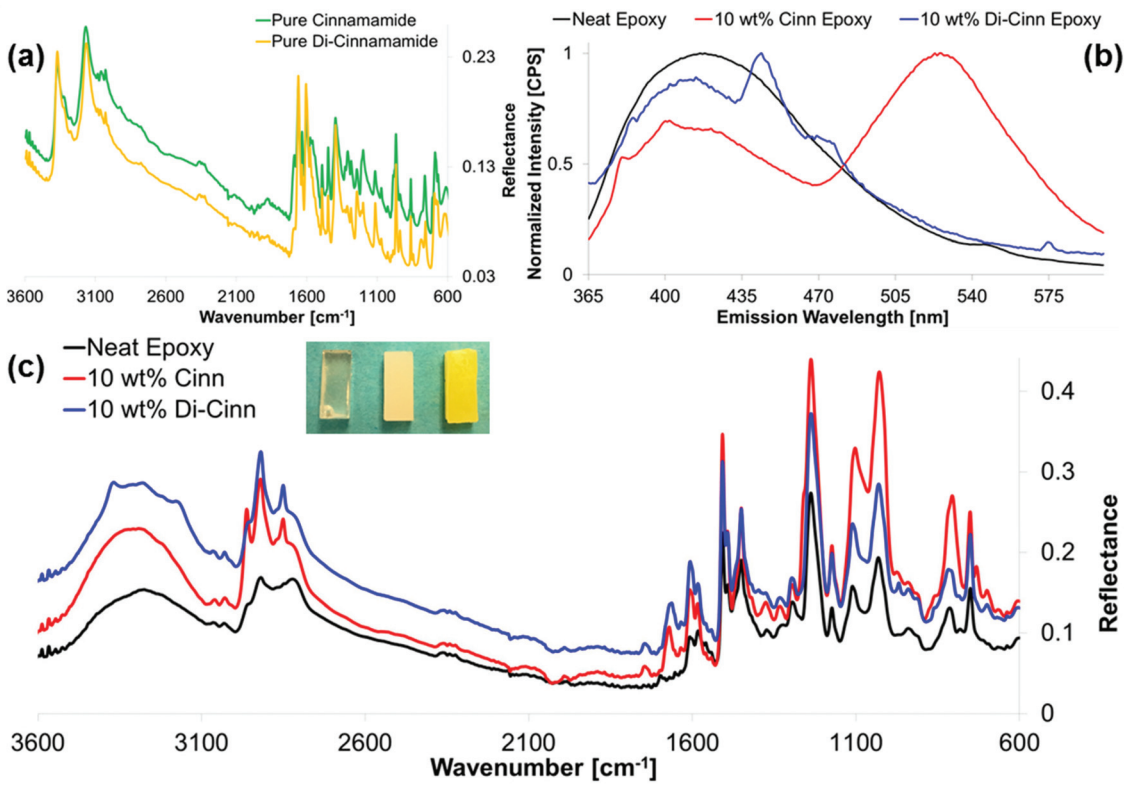

Fig. 2 (a) ATR-FTIR spectra comparing cinnamamide (green) with di-cinnamamide (orange). (b) Emission spectra the neat epoxy (black), 10 wt% Cinn epoxy (red), 10 wt% Di-Cinn epoxy (blue) for an excitation wavelength of 350 nm. (c) ATR-FTIR spectra comparing the neat epoxy (black), with the 10 wt% Cinn epoxy (red) and 10 wt% Di-Cinn epoxy (blue), with the inset image showing the neat epoxy, the 10 wt% Di-Cinn epoxy, and the 10 wt% Cinn epoxy samples (from left to right).

mechanophore–resin reaction, with more defined evidence from the spectra at the smaller wavenumbers.

A macroscopic viewing of the functionalization is additionally seen in the inset images of Fig. 1b and c, which shows diluted reaction solution aliquots taken at 0, 1, 2, 3, and 4 h from left to right. At 0 h, before the reaction occurred, both Cinn and Di-Cinn reaction solutions were colorless, due to the solubility of both in dichloromethane. However, after only 1 h of reaction, cinnamamide reaction solution turned fluorescent opaque yellow, with the amount of yellow color increasing as the reaction proceeded. This color change is a visible signal of the resin–mechanophore functionalization, as the UV fluorescence of the cinnamamide is shifted to the longer visible wavelengths upon reaction with the large resin molecules. The di-cinnamamide reaction solution turned white and opaque as the reaction proceeded, which is expected to be the functionalized di-cinnamamide resin that should not have intrinsic fluorescence unless the dimers are broken under a mechanical stress.

The ATR-FTIR spectra of the pure cinnamamide crystals and di-cinnamamide powder can been seen in Fig. 2a, with the important primary amine hydrogen peaks at 3367 and 3157 cm^{-1}. Other defining peaks for the spectrum include the C═O carbonyl stretch, and various aromatic peaks, below 1700 cm^{-1}. Fig. 2c shows the resulting ATR-FTIR spectra for the neat epoxy, and the 10 wt% Cinn and 10 wt% Di-Cinn epoxy nanocomposites, with the Cinn composite having undergone UV curing. A macroscopic image of the epoxy samples on a light blue background can be seen in the inset of Fig. 2c, with the neat epoxy being translucent, the 10 wt% Di-Cinn epoxy being opaque white, and the 10 wt% Cinn epoxy being opaque yellow; the fluorescent yellow color of the Cinn composite being a visual indicator of its intrinsic fluorescence even before damage is applied, due to the lower amount of cyclobutane formation as a result of UV dimerization in the curing epoxy mixture. In the neat and composite epoxy FTIR spectra, the clear, broad –OH peak near 3300 cm^{-1} is present, due to the opening of the epoxide rings during epoxy curing. It should be noted that the 10 wt% Di-Cinn composite spectrum exhibits flattening out of this peak and a small peak at 3350 cm^{-1} compared to the other spectra, which can be evidence that the Di-Cinn composite still retains some of its amine hydrogens, likely only moving from the primary amine to the secondary amine form, due to the increase in the steric hindrance in the Di-Cinn-DGEBF reaction, as compared to the Cinn-DGEBF reaction. The smooth nature of the Cinn peak in the region implies that all or most of its amine hydrogens were removed during its reaction with the resin. This difference in the bonding between Cinn and Di-Cinn with the epoxy matrix can result in differences in the mechanochemical response discussed below. Compared to the neat epoxy, the Cinn and Di-Cinn composites exhibit additional peaks at 2916 and 2846 cm^{-1}, with an additional peak for Cinn at 2941 cm^{-1}. These peaks are representative of the newly present aromatic and alkane C–H bonds in the nanocomposites. Other important functional group peaks can be seen below 1700 cm^{-1}, and are similar to the peaks discussed above as shown in Fig. 1. Overall, from the ATR-FTIR spectra of the reaction between cinnamamide and di-cinnamamide and DGEBF, along with the spectra for the final nanocomposites, there is sufficient evidence for the covalent grafting of the mechanophore units into the thermoset epoxy network.

Fig. 2b shows the comparison of the fluorescent emission for the neat epoxy, and the Cinn and Di-Cinn composites under 350 nm excitation, with each curve normalized to its maximum emission. Both neat and Di-Cinn epoxy samples have similar emission with the maximum between 370 and 470 nm, while the Cinn epoxy has its maximum emission at the higher wavelength range of 500 to 600 nm. This confirms the macroscopic fluorescence visualization of the composite samples mentioned above, and as the emission wavelengths gathered in the subsequent fluorescence microscopy imaging are between 500 and 550 nm, it is expected that the neat and Di-Cinn samples will have a much lower intrinsic or baseline fluorescence as compared to the Cinn samples.

3.2. Effects of mechanophore-grafting on the nanocomposite material properties

As the newly formed nanocomposites feature covalent incorporation of the mechanophore units, it is desired to evaluate their effect on the material properties. Differential Scanning Calorimetry (DSC) was used to determine the glass transition temperature (T_g) of the neat and mechanophore incorporated samples. A representative DSC scan for the neat epoxy can be seen in Fig. 3a, with scans for the 10 wt% Cinn and Di-Cinn composites shown in Fig. 3b. The T_g values were calculated at the step transition in the curves with the TA Universal Analysis software. The average T_g values over 4 runs were 47.85 ± 3.01 °C, 41.46 ± 0.82 °C, and 42.28 ± 1.22 °C, for the neat, 10 wt% Cinn, and 10 wt% Di-Cinn samples, respectively. This results in a decrease of the T_g from the neat of approximately

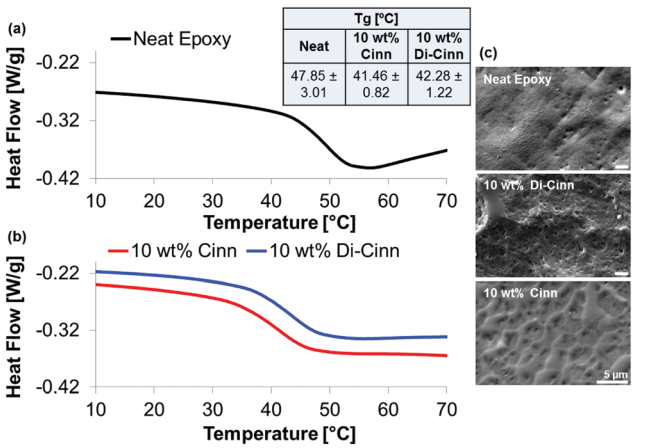

Fig. 3 Representative DSC scans showing the glass transition for the (a) neat epoxy (black) and the (b) 10 wt% Cinn and Di-Cinn epoxy composites (red and blue, respectively), with the resulting T_g values (as an average of 4 runs) in the inset on the top right. (c) Representative SEM images showing the epoxy surfaces.

6 °C for both the mechanophore nanocomposites. This T_g decrease can be expected as the newly formed mechanophore bonds are not as thermally stable as the neat epoxy network, however a 6 °C lowering is relatively low compared to other studies regarding mechanophore incorporated composites. Fig. 3c shows the SEM images of the neat and composite samples, with some difference in the surface morphology observed, but not a significant enough different to imply phase separation. Additionally, as the DSC scan only reported one T_g, it is additionally confirmed that the mechanophore units are successfully grafted and are miscible with the matrix.

Fig. 4 shows representative Thermogravimetric Analysis (TGA) for the samples, with the corresponding Differential Thermal Gravimetry (DTG) curves in the left inset. These tests were run under nitrogen to prevent weight loss due to oxidation, and thus purely capture the thermal decomposition of the bonds within the epoxy samples. The main decomposition temperatures (T_d) were found *via* the tallest peaks in the DTG curves, and were 349.10 ± 3.77 °C, 363.91 ± 1.72 °C, and 369.09 ± 2.26 °C, for the neat, 10 wt% Cinn, and 10 wt% Di-Cinn samples, respectively. The addition of the mechanophore did shift the main decomposition temperature higher than the neat by approximately 15 to 20 °C, for the Cinn and Di-Cinn mechanophores, respectively.

However, there is a notable weight loss in the mechanophore containing composites of approximately 20% from 90 to 310 °C, followed by the main degradation. From the DTG curves, it also appears that there are two small peaks before the main T_d at 120 and 236 °C. The T_d values of the pure cinnamamide and di-cinnamamide (prior to embedding) were found to be 249.15 ± 1.24 °C and 251.68 ± 7.45 °C, respectively, and occurred in one sharp decomposition step, with little to no weight loss before 200 °C. This degradation of the mechanophores help to explain the second slight decomposition step near 236 °C in the composites, thus the first small decomposition step near 120 °C is likely due to the breaking of the bonds between the mechanophore units and the epoxy matrix. This step is more pronounced in the Di-Cinn sample, and is likely due to the lessened conjugation of the dimer with the matrix initially, due to the di-substitution of the dimers, rather than the full substitution seen with the cinnamamide–resin reaction.

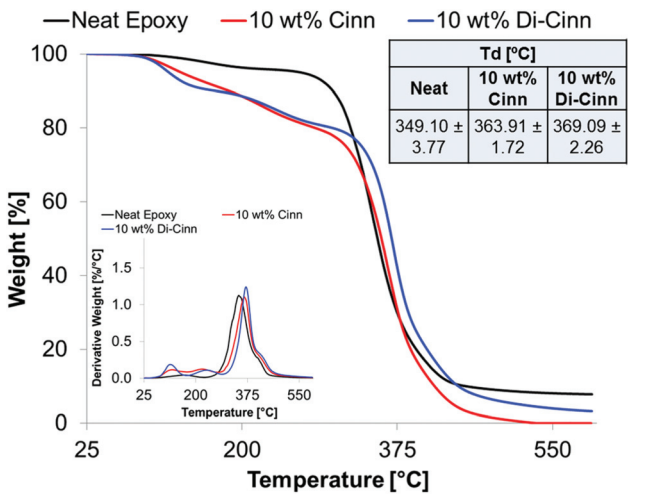

Fig. 4 Representative TGA curves showing the decomposition of neat epoxy (black), and the 10 wt% Cinn (red) and 10 wt% Di-Cinn (blue) epoxy composites, with the resulting major T_d values (as an average of 4 runs) in the inset on the top right. The left inset shows the respective DTG curves to determine the T_d values.

In addition to utilizing DSC to determine the T_g values, Dynamic Mechanical Analysis (DMA) can be used, with representative curves seen in Fig. 5. The peak of the tan delta (tan δ) curve in DMA is used to determine the T_g value for the sample, with tan δ being defined as the ratio between the loss and storage moduli. From DMA, the T_g values over 4 runs of each sample were 60.83 ± 1.50 °C, 52.66 ± 2.80 °C, and 52.23 ± 2.05 °C, for the neat epoxy, and the 10 wt% cinnamamide and di-cinnamamide composites, respectively. This makes for a lowering of the T_g from the neat by about 9 °C for the mechanophore grafted samples, with the mechanophore grafted samples having statistically similar T_g values. It should be noted that this decrease is slightly more than what was seen with DSC, and overall, all of the T_g values are greater with DMA compared to that of DSC. These results can be hypothesized to be from the mechanical determination of the T_g in DMA, rather than the thermal determination in DSC.

DMA can also be used to calculate the crosslink density for a given sample, according to the theory of rubber elasticity,[52] $\rho_{xl} = \frac{G'}{3RT}$, where ρ_{xl} is the crosslink density expressed in moles of elastically effective network chains per cm^3 of sample, G' is the rubbery plateau modulus, R is the gas constant, and T is the absolute temperature at which the rubbery plateau storage modulus is determined. The crosslink densities were thus calculated to be 0.73 ± 0.01 × 10^3 mol cm^{-3}, 0.55 ± 0.02 × 10^3 mol cm^{-3}, and 0.63 ± 0.09 × 10^3 mol cm^{-3} for the neat epoxy, and the 10 wt% cinnamamide and di-cinnamamide composites, respectively. Similar to the other thermomechanical property comparisons, the neat epoxy was expected to be more highly crosslinked than either mechanophore containing composites.

3.3. Compressive mechanochemical activation and observed fluorescent response

To evaluate the mechanochemical response of the mechanophore-grafted nanocomposites, compression tests were used to apply repeatable and quantifiable damage to the thermoset samples. From these compression tests, stress–strain curves were obtained for each of the different sample types, as seen in Fig. 6. The Young's modulus values were calculated from the slope in the linear elastic region of the curves, and were found to be 2.21 ± 0.01 GPa, 1.36 ± 0.09 GPa, and 1.89 ± 0.09 GPa for the neat epoxy, 10 wt% Cinn and 10 wt% Di-Cinn epoxy composites, respectively. Thus, there was a notable decrease in the Young's modulus upon 10 wt% cinnamamide mechanophore incorporation, but the use of 10 wt% di-cinnamamide notably increases the Young's modulus value. Similarly, the yield strength values were 95.61 ± 1.26 MPa,

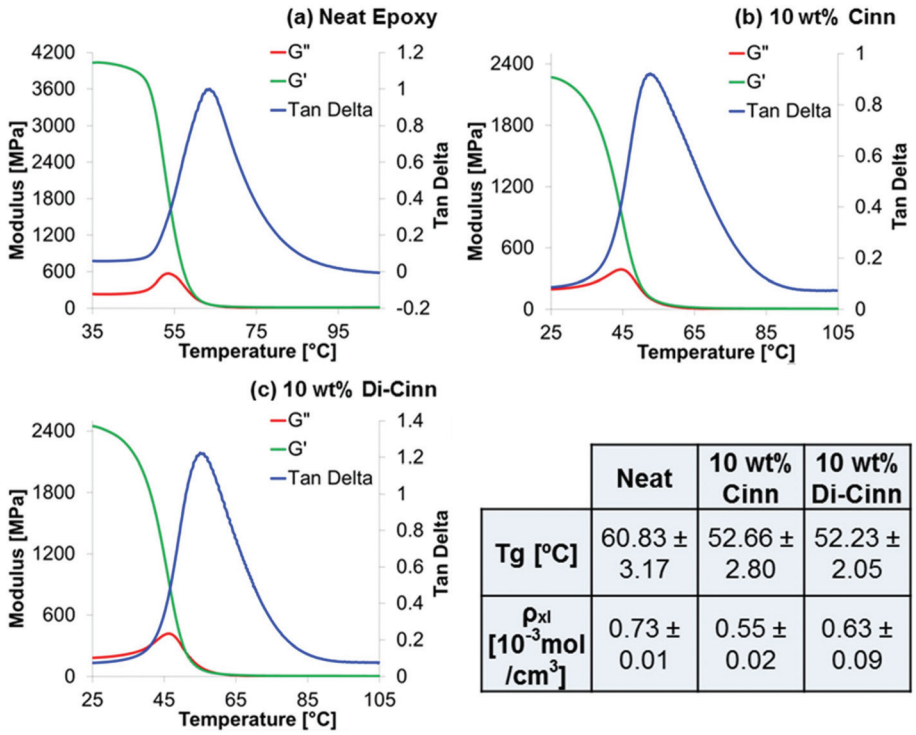

	Neat	10 wt% Cinn	10 wt% Di-Cinn
Tg [°C]	60.83 ± 3.17	52.66 ± 2.80	52.23 ± 2.05
ρ_{xl} [10^{-3}mol /cm^3]	0.73 ± 0.01	0.55 ± 0.02	0.63 ± 0.09

Fig. 5 DMA curves showing the storage modulus (G', green), loss modulus (G'', red), and tan delta (blue) of the (a) neat epoxy, (b) 10 wt% cinnamamide composite, and (c) 10 wt% di-cinnamamide composite, respectively. The inset table shows the average T_g and ρ_{xl} of the samples determined from the DMA curves.

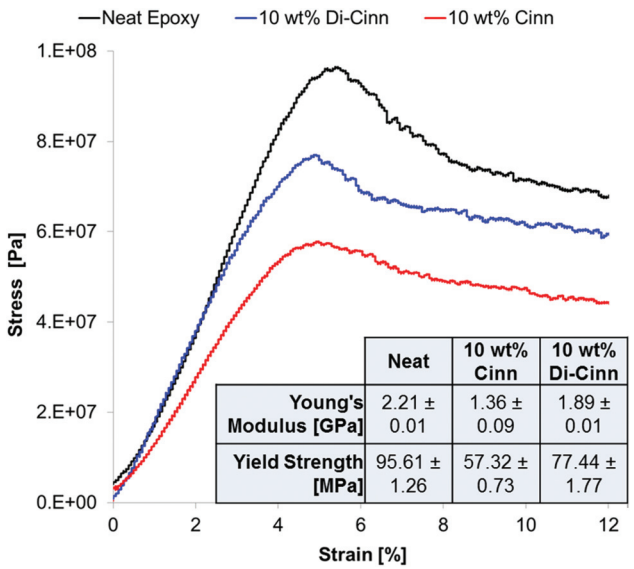

	Neat	10 wt% Cinn	10 wt% Di-Cinn
Young's Modulus [GPa]	2.21 ± 0.01	1.36 ± 0.09	1.89 ± 0.01
Yield Strength [MPa]	95.61 ± 1.26	57.32 ± 0.73	77.44 ± 1.77

Fig. 6 Stress–strain curves for the neat epoxy (black), and the 10 wt% Cinn (red) and 10 wt% Di-Cinn (blue) epoxy composites, with the lower right inset showing the resulting Young's modulus and yield strength values.

57.32 ± 0.73 MPa, and 77.44 ± 1.77 MPa for the neat, 10 wt% Cinn, and 10 wt% Di-Cinn epoxy samples, respectively. This increase in the mechanical properties when Di-Cinn is used as opposed to Cinn is, again, likely due to the higher crosslink density in the Di-Cinn composites from the mechanophore cyclobutane dimers being formed prior to incorporation into the epoxy mixture.

Fluorescence microscopy was then used in tandem with the compression tests to evaluate the fluorescent response of the self-sensing thermoset network composites, with fluorescence images taken at the strain values of 0, 2, 4, 6, 10, and 15%. From the compression test curves, 0% strain is the baseline value prior to compression, while 2% and 4% strain are in the elastic region, with 4% immediately before the yield point. 6% strain is immediately after the yield point, and 10 and 15% strain are well into the plastic region.

The representative images for the selected strain values for the 10 wt% Cinn and Di-Cinn epoxy nanocomposites can be seen in Fig. 7a and b, respectively. These images were taken under excitation of 340–380 nm UV light, capturing the fluorescent emission between 500–550 nm. The raw 8-bit gray scale fluorescence images were pseudocolored green and the brightness and contrast were increased by 40% for better visualization and are shown in Fig. 7. It can be clearly seen that the 10 wt% Cinn composite has a much higher fluorescent emission overall compared to the 10 wt% Di-Cinn composite, which was further confirmed by the macroscale visualization of the samples and the fluorometer data. This reinforces the hypothesis that the cinnamamide groups in this composite are much less crosslinked, and less mechanically sensitive cyclobutane units are formed, than when the di-cinnamamide is incorporated into the epoxy. For both of the composites

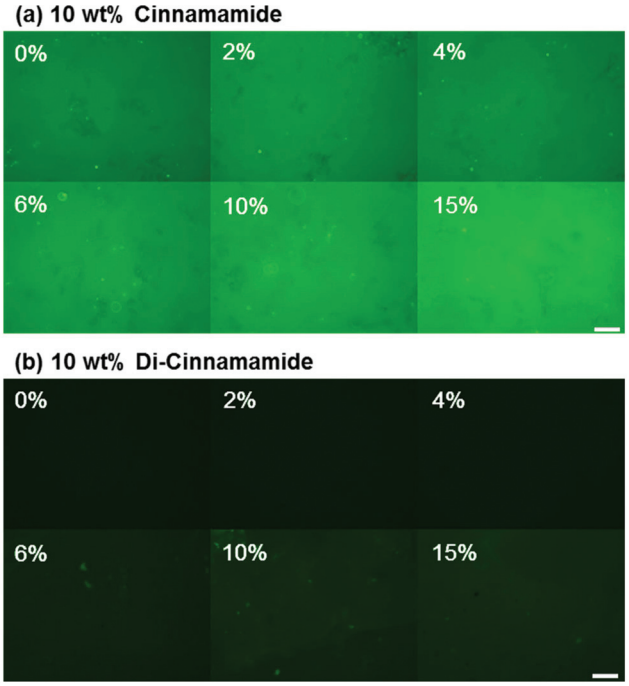

Fig. 7 Representative fluorescence images for the mechanophore-embedded epoxy composites identifying the strain values for which the images were taken, for (a) 10 wt% cinnamamide and (b) 10 wt% di-cinnamamide. Scale bars are 50 μm. The images were pseudocolored green and the brightness and contrast were increased by 40% to enhance the visual analysis of the images.

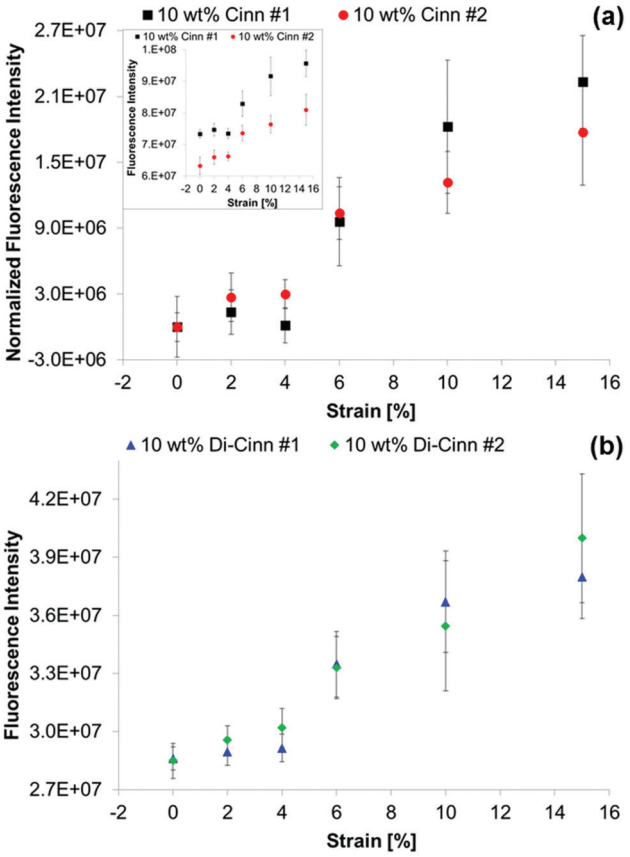

Fig. 8 Average fluorescence intensity values for each strain calculated *via* ImageJ from the obtained fluorescence microscopy images, with each point being an average of 20 images and 2 samples per batch. (a) Upper left inset shows the raw fluorescence intensity data for 2 batches of the 10 wt% Cinn epoxy composite, while the main image shows the overlay of the two curves by normalizing the intensity to the 0% strain value. (b) Raw fluorescence intensity data for 2 batches of the 10 wt% Di-Cinn epoxy composite, showing good agreement between the batches.

studied, there is an overall increase in the fluorescence with an increase of the strain applied, however, there is not a clear difference between the 0, 2, and 4% strains, which would be required for damage precursor detection. There seems to be a noticeable difference between the 4 and 6% strain values, thus quantification of the fluorescence *via* ImageJ was performed to analyze the phenomenon further.

For each sample analyzed, ten fluorescence images were taken representative of the sample face and the ImageJ software calculated average fluorescence intensity values for each image. For each composite batch made, two samples for each strain percentage would be analyzed, thus each point shown in Fig. 8 is an average of 20 images. The upper left inset of Fig. 8 shows the raw fluorescence intensity data for 2 batches of the 10 wt% Cinn epoxy composite, which were found to have slightly different fluorescence intensity values initially, likely due to the variation in the UV curing of the epoxy samples, which could be attributed to the light penetration depth, among other factors. However, when the curves are overlaid by normalizing the intensities to the 0% strain value, there is good agreement in the shape of the curve and the strains at which damage can be detected, as seen in the main image of Fig. 8a. There is no significant difference in the fluorescence intensity values between the 0, 2, and 4% strains, but there is a marked increase in the fluorescence intensity at the 6% strain mark, which is immediately after the yield point, and can serve as early damage detection. The 10 and 15% strain values show a further increase in the intensity with the applied strain, as expected.

Similarly, Fig. 8b shows the raw fluorescence intensity data for two batches of the 10 wt% Di-Cinn epoxy composites, with no normalization, showing good agreement between the batches. Both batches have nearly identical starting fluorescences, and there is not a significant increase in the intensity for the batches for 2 or 4% strain. However, akin to the 10% Cinn composite batches, there is a marked statistical increase in the fluorescence at the 6% strain, with the intensity increasing with the application of 10 or 15% strain. This early damage detection at 6% strain reinforces our previous work, which involved photodimerization of cinnamoyl functional groups to create cyclobutane stress-sensing moieties within polymer blends of crosslinked-cyclobutane containing polymers and epoxy.[46] Thus, despite the covalent incorporation into the epoxy network, there is not an improvement in the occurrence of the fluorescent response, likely due to the limitation of the cinnamoyl chemistry in terms of its fluorescence

quantum yield. This shows that Cinn or Di-Cinn can be covalently grafted into a thermoset epoxy network and can additionally be used as a stress-responsive mechanophore *via* fluorescent signal generation, and that applying increasing strain increases the fluorescence emission, due to the breaking of the formed cyclobutane dimers, causing reversion to the fluorescent monomeric form.

4. Conclusion

Mechanochemistry is a relatively new and exciting field, and the pervasive nature of damage makes it an important one, with thermoset composites being rarely studied for stress sensing. In this work, we prepared novel, grafted, covalently-bonded, self-sensing mechanophore-embedded thermoset network nanocomposites. This study has the potential to open new directions to polymer mechanochemistry, as while mechanophores of varying chemistries have been covalently incorporated into elastomeric and thermoplastic polymer systems, they had not yet been covalently incorporated into a thermoset network polymer. The mechanophore precursor chosen was cinnamamide, as its amine group can covalently bond to the epoxy resin chosen, in a similar manner to the crosslinking of the resin with the chosen hardener in the neat epoxy system. Cinnamamide was known to be able to form a cyclobutane type dimer (di-cinnamamide) under UV photoirradiation *via* [2 + 2] cycloaddition. Thus two routes were studied for the mechanophore covalent incorporation into an epoxy matrix, the first being the reaction of the cinnamamide mechanophore precursor with the epoxy resin to ensure covalent bond formation, with subsequent hardener addition. The epoxy mixture was then UV cured so that the cyclobutane mechanophore units could be formed *via* photodimerization, while the conventional resin-hardener curing took place. The second route was to first form di-cinnamamide in solution under UV light, then to react it with the epoxy resin, with subsequent hardener addition and conventional epoxy bond formation. In this second method, there were more cyclobutane rings present in the final nanocomposite, as di-cinnamamide was theoretically 100% dimerized prior to addition, and this thus affected the resulting material properties of the composites. The chemistry of the covalent bonding between the mechanophore units and the epoxy constituents was confirmed *via* an extensive FTIR study, and its effect on the composite material properties including the T_g, decomposition temperature, crosslink density, Young's modulus, and yield strength was studied. By these methods, it was determined that the amount of cyclobutane bond generation and the mechanophore–resin substitution amount determined the resulting material and sensing properties. Compression tests were used to apply damage to the mechanophore-embedded networks, and fluorescent early damage detection occurred immediately after the yield point for both the cinnamamide and di-cinnamamide systems. Overall, both the routes of mechanophore incorporation were successful in creating grafted, self-sensing thermoset network composites, which were capable of early damage detection *via* fluorescence emission.

Acknowledgements

We would like to acknowledge the financial support from the Army Research Office, Grant Number W911NF1510072, Program Manager Dr David Stepp, and student support from the National Science Foundation Graduate Research Fellowship Program, the ARCS Foundation, and the Fulton Undergraduate Research Initiative. We would also like to acknowledge Dr Bin Mu's Laboratory, the W. M. Keck Bioimaging Laboratory, the LeRoy Eyring Center for Solid State Science, and the Adaptive Intelligent Materials & Systems Center, all at Arizona State University, for the use of their facilities.

References

1 T. Rojac, P. Segedin and M. Kosec, Using Infrared Spectroscopy to Identify New Amorphous Phases – A Case Study of Carbonato Complex Formed by Mechanochemical Processing, in *Infrared Spectroscopy – Materials Science, Engineering and Technology*, InTech, 2012, p. 13.
2 X. Liu, Y. Shao, Y. Zhang, G. Meng, T. Zhang and F. Wang, *Corros. Sci.*, 2015, **90**, 451–462.
3 S. L. James, C. J. Adams, C. Bolm, D. Braga, P. Collier, T. Friscic, F. Grepioni, K. D. M. Harris, G. Hyett, W. Jones, A. Krebs, J. Mack, L. Maini, A. G. Orpen, I. P. Parkin, W. C. Shearouse, J. W. Steed and D. C. Waddell, *Chem. Soc. Rev.*, 2012, **41**, 413–447.
4 C. R. Hickenboth, J. S. Moore, S. R. White, N. R. Sottos, J. Baudry and S. R. Wilson, *Nature*, 2007, **446**, 423–427.
5 A. L. Black, J. M. Lenhardt and S. L. Craig, *J. Mater. Chem.*, 2011, **21**, 1655–1663.
6 D. A. Davis, A. Hamilton, J. Yang, L. D. Cremar, D. Van Gough, S. L. Potisek, M. T. Ong, P. V. Braun, T. J. Martinez, S. R. White, J. S. Moore and N. R. Sottos, *Nature*, 2009, **459**, 68–72.
7 M. N. Silberstein, K. Min, L. D. Cremar, C. M. Degen, T. J. Martinez, N. R. Aluru, S. R. White and N. R. Sottos, *J. Appl. Phys.*, 2013, **114**, 023504.
8 J. N. Brantley, K. M. Wiggins and C. W. Bielawski, *Polym. Int.*, 2013, **62**, 2–12.
9 S. L. Potisek, D. A. Davis, N. R. Sottos, S. R. White and J. S. Moore, *J. Am. Chem. Soc.*, 2007, **129**, 13808–13809.
10 M. B. Larsen and A. J. Boydston, *J. Am. Chem. Soc.*, 2013, **135**, 8189–8192.
11 M. K. Beyer and H. Clausen-Schaumann, *Chem. Rev.*, 2005, **105**, 2921–2948.
12 T. Ikawa, T. Shiga and A. Okada, *J. Appl. Polym. Sci.*, 1997, **66**, 1569–1573.
13 D. R. T. Roberts and S. J. Holder, *J. Mater. Chem.*, 2011, **21**, 8256–8268.
14 D. Olmos, A. Aznar, J. Gonzalez-Benito and J. Baselga, *J. Mater. Process. Technol.*, 2003, **143**, 495–500.

15 J. N. Brantley, K. M. Wiggins and C. W. Bielawski, *Polym. Int.*, 2013, **62**, 2–12.
16 J. Li, C. Nagamani and J. S. Moore, *Acc. Chem. Res.*, 2015, **48**, 2181–2190.
17 N. R. Sottos, *Nat. Chem.*, 2014, **6**, 381–383.
18 C. M. Kingsbury, P. A. May, D. A. Davis, S. R. White, J. S. Moore and N. R. Sottos, *J. Mater. Chem.*, 2011, **21**, 8381–8388.
19 A. N. Celestine, B. A. Beiermann, P. A. May, J. S. Moore, N. R. Sottos and S. R. White, *Polymer*, 2014, **55**, 4164–4171.
20 G. R. Gossweiler, G. B. Hewage, G. Soriano, Q. Wang, G. W. Welshofer, X. Zhao and S. L. Craig, *ACS Macro Lett.*, 2014, **3**, 216–219.
21 T. Nakamura, K. Takagi, M. Itoh, K. Fujita, H. Katsu, T. Imae and Y. Sawaki, *J. Chem. Soc., Perkin Trans. 2*, 1997, 2751–2755.
22 K. Takagi, M. Itoh, H. Usami, T. Imae and Y. Sawaki, *J. Chem. Soc., Perkin Trans. 2*, 1994, 1003–1009.
23 S. Cho, J. Kim and C. Chung, *Sens. Actuators, B*, 2008, **134**, 822–825.
24 S. Cho, J. Kim and C. Chung, *J. Nanosci. Nanotechnol.*, 2010, **10**, 6972–6976.
25 C. Chung, Y. Roh, S. Cho and J. Kim, *Chem. Mater.*, 2004, **16**, 3982–3984.
26 N. Oya, P. Sukarsaatmadja, K. Ishida and N. Yoshie, *Polym. J.*, 2012, **44**, 724–729.
27 M. J. Kryger, M. T. Ong, S. A. Odom, N. R. Sottos, S. R. White, T. J. Martinez and J. S. Moore, *J. Am. Chem. Soc.*, 2010, **132**, 4558–4559.
28 P. Cintas and G. Cravotto, *Nat. Chem.*, 2012, **4**, 77–78.
29 M. J. Kryger, A. M. Munaretto and J. S. Moore, *J. Am. Chem. Soc.*, 2011, **133**, 18992–18998.
30 Y. Zheng, Z. Shen, S. Ma, C. Cai, X. Zhao and Y. Xing, *J. Hazard. Mater.*, 2009, **170**, 978–982.
31 B. Jensen, R. Bryant, J. Smith and P. Hergenrother, *J. Adhes.*, 1995, **54**, 57–66.
32 S. G. Kulkarni, X. Gao, S. E. Horner, J. Q. Zheng and N. V. David, *Compos. Struct.*, 2013, **101**, 313–331.
33 U. K. Vaidya and K. K. Chawla, *Int. Mater. Rev.*, 2008, **53**, 185–218.
34 E. Girard-Reydet, V. Vicard, J. Pascault and H. Sautereau, *J. Appl. Polym. Sci.*, 1997, **65**, 2433–2445.
35 J. Gillham, *Polym. Int.*, 1997, **44**, 262–276.
36 M. Zako and N. Takano, *J. Intell. Mater. Syst. Struct.*, 1999, **10**, 836–841.
37 B. A. Beiermann, D. A. Davis, S. L. B. Kramer, J. S. Moore, N. R. Sottos and S. R. White, *J. Mater. Chem.*, 2011, **21**, 8443–8447.
38 M. M. Caruso, D. A. Davis, Q. Shen, S. A. Odom, N. R. Sottos, S. R. White and J. S. Moore, *Chem. Rev.*, 2009, **109**, 5755–5798.
39 N. Yoshie, S. Saito and N. Oya, *Polymer*, 2011, **52**, 6074–6079.
40 V. K. Johns, Z. Shi, W. Dang, M. D. McInnis, Y. Weng and Y. Liao, *J. Phys. Chem. A*, 2011, **115**, 8093–8099.
41 R. Gostl and R. P. Sijbesma, *Chem. Sci.*, 2016, **7**, 370.
42 M. A. Tasdelen, *Polym. Chem.*, 2011, **2**, 2133–2145.
43 Y. L. Liu and C. Y. Hsieh, *J. Polym. Sci., Part A: Polym. Chem.*, 2006, **44**, 905–913.
44 N. Bai, K. Saito and G. P. Simon, *Polym. Chem.*, 2013, **4**, 724–730.
45 G. Kaupp, *CrystEngComm*, 2009, **11**, 388–403.
46 J. Zou, Y. Liu, B. Shan, A. Chattopadhyay and L. L. Dai, *Smart Mater. Struct.*, 2014, **23**, 095038.
47 E. M. Nofen, J. Wickham, B. Koo, A. Chattopadhyay and L. L. Dai, *Mater. Res. Express*, 2016, **3**, 035701.
48 J. B. Lambert, *Introduction to Organic Spectroscopy*, Macmillan, New York, 1987.
49 M. Gonzalez, J. Carlos and J. Baselg, *Infrared Spectroscopy - Materials Science, Engineering and Technology*, 2012.
50 H. B. Henbest, G. D. Meakins, B. Nicholls and K. J. Taylor, *J. Chem. Soc.*, 1957, 1459–1462.
51 Y. M. Evtushenko, V. M. Ivanov and B. E. Zaitsev, *J. Anal. Chem.*, 2003, **58**, 347–350.
52 L. E. Nielsen, *J. Macromol. Sci., Rev. Macromol. Chem.*, 1969, **3**, 69–103.